UNSTEADY PRESSURE CHARACTERISTICS OF MODIFIED RECTANGULAR CROSS-SECTIONS

Trein, Cristiano Augusto[1]; Shirato, Hiromichi [2] and Matsumoto, Masaru [3]

[1] *Graduate Student, Bridge and Wind Eng. Lab., Kyoto University, ctrein@cristianotrein.com*

[2] *Professor, Department of Civil Eng., Kyoto University, shirato@brdgeng.gee.kyoto-u.ac.jp*

[3] *Professor Emeritus, Department of Civil Eng., Kyoto University, matsu@brdgeng.gee.kyoto-u.ac.jp*

ABSTRACT

In this study, empirical equations to be used in the estimation of the unsteady pressure characteristics of rectangular cylinders are investigated, as part of the development of a bridge deck design framework based on the manipulation of these characteristics. Even by using different leading edges it could be verified that the phase difference distribution of such a bluff body can be approximated by a sinusoidal equation, the amplitude distribution follows a Weibull distribution and both are interrelated by the wave length developed along the body's surface. The efficacy of the formulations could be confirmed through wind tunnel tests.

KEYWORDS: *unsteady pressure characteristics, rectangular cross-sections, aerodynamic derivatives*

Introduction

The design process of long-span bridges is mostly based on wind tunnel test campaigns, in which through a trial and error approach an initial cross-section is proposed and improvements are tried until the stability requirements are reached. Concerning flutter stability this has been done based on the control of the aerodynamic derivatives, in a manner that the efficiency of geometric improvements has been related to the impacts they have on these derivatives. Exact generic relationships between geometry and aerodynamic derivatives are still not available so that this process is still very empiric.

Since the aerodynamic derivatives are a representation of the unsteady pressure characteristics along the deck, a more rational approach would be based on the judicious manipulation of these characteristics, instead of focusing directly on the derivatives. However, relationships between geometry and these characteristics can only be obtained by detailed pressure measurements, not usually performed, or by CFD simulations, still time consuming.

In this sense, the systematization of a design framework based on the direct manipulation of the unsteady pressure characteristics of bridge decks through geometric improvements could be proposed if prompt formulations to be used in the estimation of the unsteady pressure characteristics of such structures existed. By using such formulations the designer would have the chance to, *a priori*, have an insight on the tendency a bridge deck geometry would have to present flutter or not, making the necessary geometric improvements before going to wind tunnel tests, which would be reserved to a more advanced stage.

As an initial step towards the proposition of such a framework and as a proof of concept, an investigation based on wind tunnel experiments is presented. Universal equations for the estimation of the unsteady pressure characteristics of rectangular cylinders are proposed and checked, with the objective of showing that even by using different leading edges, simple empirical equations can provide good approximations for these characteristics, provided the right coefficients are used.

Approach

The investigations were carried out based on wind tunnel test results, which were conducted by using rectangular cylinders with side ratio B/D=20 in four different configurations: no fairing in the leading edge (NF), *corner up* leading edge (CU), *corner down* leading edge (CD) and semi-circular leading edge (SC), Fig.1.

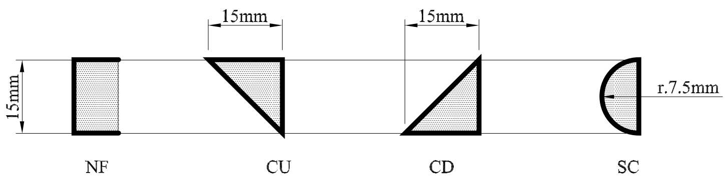

Figure 1: Leading edges

The wind tunnel used was a room-circuit Eiffel type, with working section of 1.8m height by 1.0m width, and the models were instrumented with 30 equidistant pressure taps, aligned in the widthwise direction in their center. The pressure measurements were performed in smooth flow with turbulence less than 0.5% through forced heaving/torsional 1-DOF oscillation method, with frequency f=2Hz, torsional amplitude 2φ=4 deg. and heaving amplitude 2η=20mm. The results, Fig 2-5, are expressed by the amplitude of the unsteady pressures normalized by the dynamic pressure of the flow, $\tilde{C}p$, and the phase difference Ψ between the maximum relative angle of attack and negative peak of surface pressure.

From a qualitatively point of view, all configurations present similar patterns, more or less "deformed" according to the leading edge and to the reduced wind velocity; also, in a major extent, similarities between torsional and heaving systems can be identified. Not only the separation of the flow near the leading edge is affected by the presence of different fairings, but also the whole development of the unsteady pressure characteristics along the body is. With the increase of the reduced wind velocity, the energy related to the flow is also increased, being translated into a broadening of the base of the $\tilde{C}p$ and Ψ distributions. This dependence can be also related to the traveling time of the vortices along the body, since the flow structure around rectangular cylinders is two-dimensionalized and the vortices shed from the leading edge are controlled by the motion, presenting lock-on patterns under proper conditions [Tamura *et al.*, 1995]. Based on that, it seems to be logical to build relationships between leading edge and the unsteady pressure characteristics developed after the detachment point. The discussions about this theme can include formulations based on Navier-Stokes, visualization of flow and a sort of complex theories and propositions, which still can not predict completely these interactions in a simple way; however, in this study the focus will be put on simple direct relationships between geometry and unsteady pressure characteristics.

By using the results presented in Fig.2-5, the following sections will deal with the proposition of empirical formulations to be used in the estimation of the phase difference Ψ and amplitude $\tilde{C}p$ distributions along the surface of bluff bodies, using a rectangular cylinder as a base geometry. The purpose of this proposition is to provide an initial framework that can be extended in the future to cover generic bridge cross-sections, to be used in the design phase of long span bridges, aiming the manipulation of the aerodynamic derivatives through the control of the unsteady pressure characteristics along the bridge deck, by using geometric improvements.

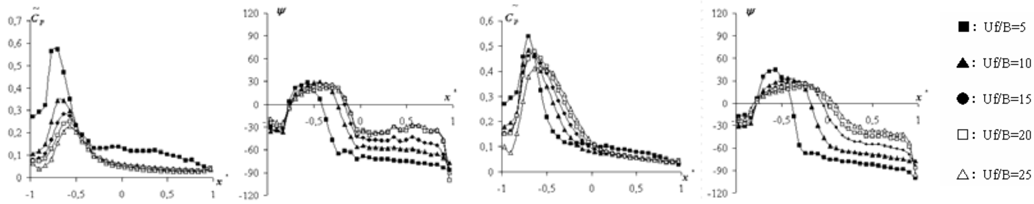

Figure 2:- Unsteady pressure characteristics of NF model (left: heaving; right: torsion)

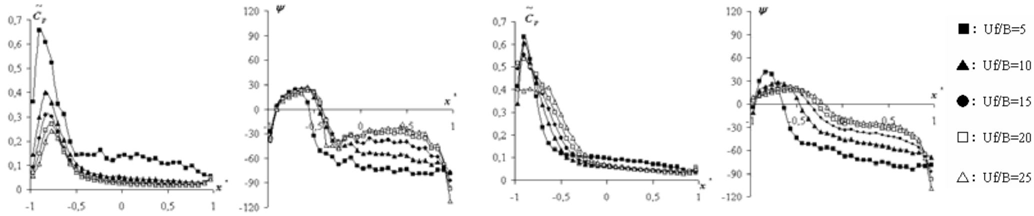

Figure 3: Unsteady pressure characteristics of CU model (left: heaving; right: torsion)

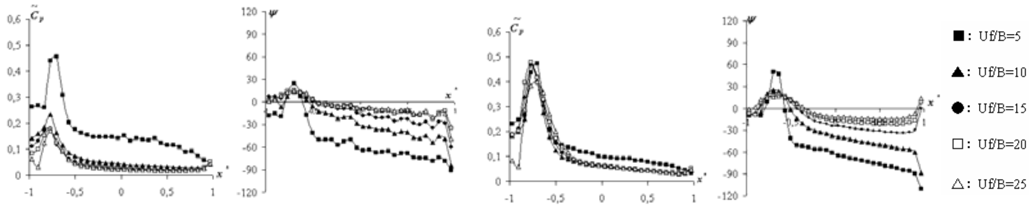

Figure 4: Unsteady pressure characteristics of CD model (left: heaving; right: torsion)

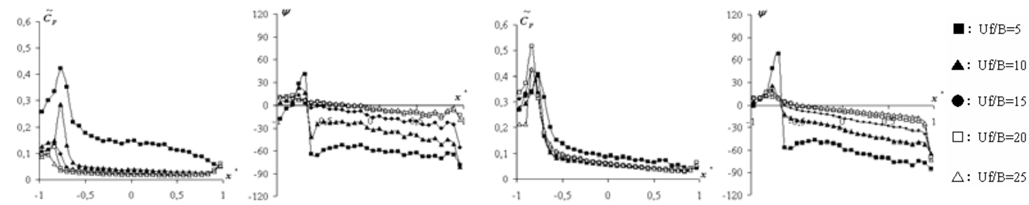

Figure 5: Unsteady pressure characteristics of SC model (left: heaving; right: torsion)

It should be mentioned that the focus of this study is on the patterns of the distributions provided by different leading edges; it is not a global assessment of the effects of the leading edge on the stability of bluff bodies. The purpose of using different leading edges was only to obtain different patterns to be analyzed, so the fact that the cases *CD* and *CU* present different unsteady pressure characteristics in the upper and in the lower surfaces due to the asymmetry of the leading edges are unimportant in this context.

Phase Difference Distribution

Observing the curves of phase difference $\Psi(x^*)$ distribution of Fig.2-5 from leading edge to trailing edge, it is perceived that a simplified description of their behavior can be tried by splitting them into two main parts: a *curvy* part, approximated by a sinusoidal equation, Eq.1, whose infection points present similar values in module; and a *steady* part, which presents constant values along its development, close to the absolute values presented by the inflection points.

$$\psi\,(x^*) = -A_{\psi}\,.\cos\left\{\varpi_{\psi}\,.(x^*+1) + \phi_{\psi}\right\} \qquad (1)$$

where: x^* is the non-dimensional location normalized by half-width b*; A_Ψ is the pseudo amplitude of the curve; ω_Ψ is the pseudo circular wave number of the curve; $\phi(x^*)$ is pseudo phase difference of the curve; "+1" is for coordinate transformation purposes.*

It is possible to identify in Fig.2-5 a dependence of the parameters A_Ψ and ϕ_Ψ on the characteristics of the leading edge, since they change among different configurations of leading edge; the same way, ω_Ψ is strongly influenced by variations of wind velocity.

In the flat plate case, the theoretical distance between successive waves in the wake vortex sheet is described by the relationship *2.π.b/k* [Silverstein and Joyner, 1939], which becomes numerically equivalent to the reduced wind velocity $U_r = U/f.b$ when normalized by the cross-section half-width *b*. In addition, it was already experimentally accounted for the existence of a relationship between the phase difference and the traveling time of the vortices on the body's surface, which is independent of both the amplitude of vibration and of the flow velocity [Kubo and Hirata, 1990]. These assumptions were verified for the models studied herein by comparing the wave half-length λ/2 obtained experimentally with the theoretical wave half-length *π.b/k*, bold line in Fig.6, and the similarities suggest that the value of *2.π.b/k* have a strong relationship with the wave length also in bluff bodies.

Since ω_Ψ represents the *pseudo circular wave number 2.π.f* in Eq.1, the multiplication of the value of the normalized wave half-length by *2.π* with a subsequent division by the wind velocity should provide the value of f_Ψ of Eq.1, which can be transformed into Eq.2.

$$\varpi_{\psi} = \frac{2.\pi}{\Delta x^*} \tag{2}$$

where: Δx is the normalized distance between the crossing points in x axis (λ/2 normalized by b)*

Using the theoretical wave length, the value of f_Ψ is calculated through Eq.3, leading to constant values throughout all the velocity range. In Fig.7 a comparison between the results obtained from Eq.2 and Eq.3 shows that the agreement between them increases with the increasing of the wind velocity, so that in the quasi-steady state they tend to be equivalents.

$$\varpi_{\psi} = \frac{\pi}{b.f} \tag{3}$$

where: f is the oscillation frequency.

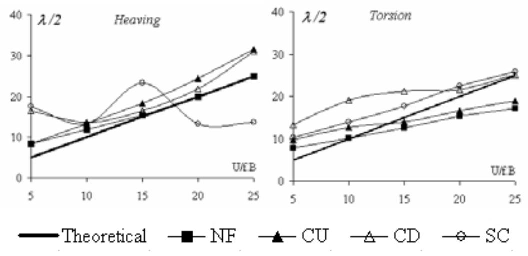

Figure 6: Wave half-length λ/2

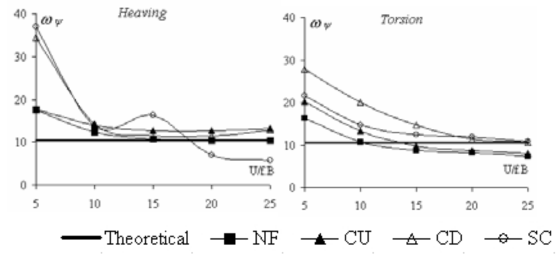

Figure 7: Pseudo circular wave number f_Ψ

In the case of the *amplitude* of the phase difference distribution, A_Ψ, the average of the absolute values at the inflection points are taken, through graphical interpolation for those distributions in which one of the peaks was missed, and Fig.8 summarizes graphically the results. Both torsional and heaving systems present similar tendencies, especially in the case of *NF*, which presents almost the same values throughout the entire range of reduced wind velocities. However, the relationships between the values obtained in each system for the same type of leading edge (development of the curves in Fig.8) vary among the different types of fairing, and with the increase of the reduced wind velocity the values seem to asymptotically approach an equilibrium state, which can be regarded as a characteristic value for each type of leading edge.

For the parameter ϕ_Ψ, the calculation was conducted by evaluating the relationship between Δx^* and the first crossing point in the *x* axis, which was regarded as a reference for ϕ_Ψ=90 degrees, also interpolating graphically the missing points. The results are presented in Fig.9, showing that this parameter presents a high sensitivity to the leading edge. Although the general tendencies presented in both systems are similar, the values assumed different ranges for all configurations of leading edges, without sharing values among themselves and looking for stabilization also in different levels.

In order to check the ability of the formulation proposed in this section in reproducing the phase difference distributions, the aerodynamic derivatives of the four cases were calculated by using the phase difference Ψ distributions obtained through Eq.1, considering Eq.2 and the parameters presented in Fig.8 and Fig.9. The real amplitude $\tilde{C}p$ of the unsteady pressure distribution was used in the calculations and the results are presented in Fig.10. The results show good agreement between wind tunnel tests data (continuous line) and the approximations through Eq.1 (dashed line), with only some minor discrepancies in the *sin* related derivatives, which showed a tendency to approach the Theodorsen equation.

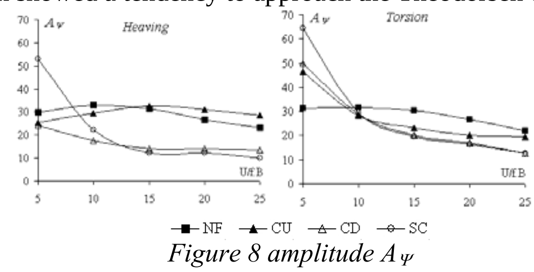

Figure 8 amplitude A_Ψ

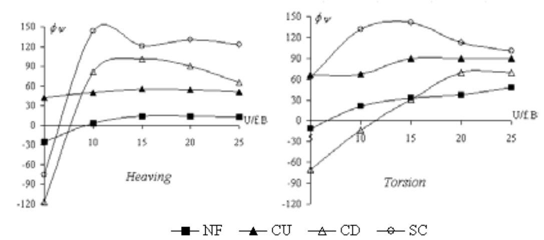

Figure 9: Phase Lag ϕ_Ψ

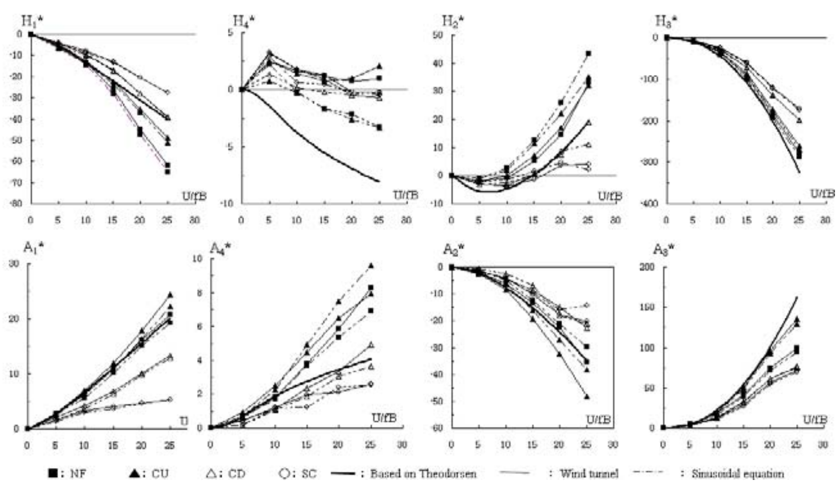

Figure 10: Derivatives - wind tunnel and sinusoidal equation

Amplitude

The amplitude of the unsteady pressure characteristics is a function of the amplitude of vibration and of the wind velocity, among other factors, being a representation of pressure fluctuations along the body surface, so that the area under its curve might be treated as a measure of part of the external work done by the fluid along one cycle of vibration in bodies in harmonic motion. For the models treated in this study, the areas under the curves of the unsteady pressure amplitude distributions were calculated for each different wind velocity and normalized by the maximum angle of attack. In Fig.11, the y axis displays this normalized area and the x axis the maximum angle of attack for which each area was obtained, showing that every type of leading edge presents a proportional relationship between area and maximum angle of attack, which is better illustrated in the heaving system (inclined lines), since for every different wind velocity different angles of attack and areas are presented. Because in the torsional motion the maximum angle of attack was kept constant (2 deg) throughout all wind velocities tested, the values for the areas are accumulated in a vertical line in x=2 deg, in concordance with the values presented by the heaving motion in x=2 deg.

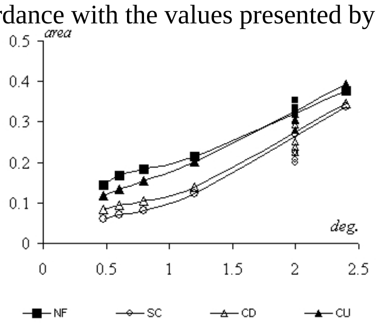

Figure 11: Normalized areas for amplitude $\tilde{C}p$ distribution

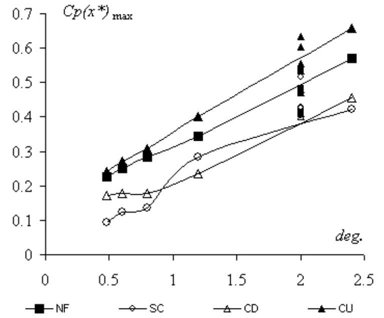

Figure 12: Relationship between maximum angle of attack and maximum $\tilde{C}p$

The existence of a relationship between maximum angle of attack and $\tilde{C}p$ in both torsional and heaving systems was already accounted for [Matsumoto, 1996], and this relationship was also verified for the cases studied herein, Fig.12, showing a pattern very similar to the one obtained in Fig.11. Based on that, it was thought to be convenient to normalize the distributions by their peak values in the search of logical relationships, generating the normalized $\tilde{C}pN$ distributions presented in Fig.13 and Fig.14, which in comparison with the phase difference distributions presented in Fig.2-5 present peaks located more upstream in almost the totality of the samples. The locations of the peaks induced by the different leading edges show different relationships with the variation of the reduced wind velocity; in the case of *NF* and *CU*, the increase of *U/f.B* promotes a displacement of the location of the peak towards downstream, for *CD* model the values are kept almost constant throughout all the velocities and for *SC* the peak is moved upstream with the increase of the wind velocity. Also, the broadening of the base of the $\tilde{C}pN$ distributions with the increase of wind velocity is an important factor to be considered.

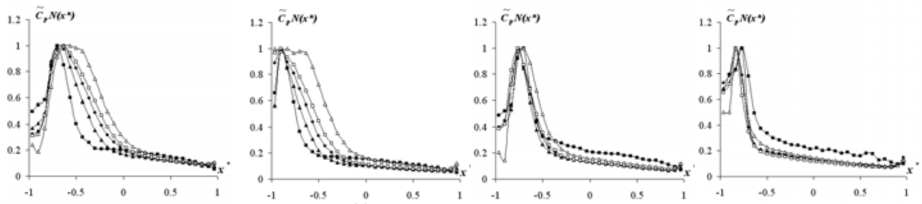

Figure 13: Normalized amplitude $\tilde{C}p$ distributions for torsional system (NF, CU, CD and SC)

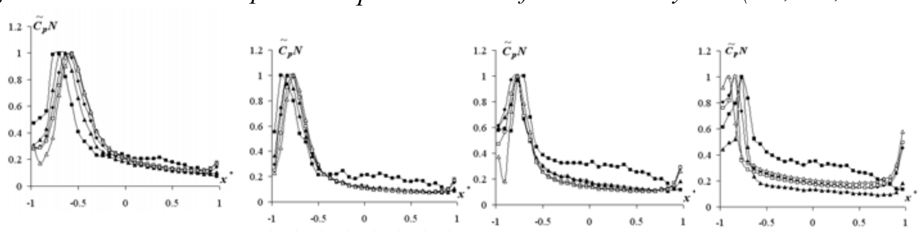

Figure 14: Normalized amplitude $\tilde{C}p$ distributions for heaving system (NF, CU, CD and SC)

Techniques of flow visualization combined with pressure measurements point out that the location of the peaks of the fluctuating pressures is strongly related to the reattachment point of the separated flow, exposing the dimension of the separation bubble, which can be finally regarded to the energy dissipated in the detachment point. In this sense it is expected that, in comparison to bluffer leading edges, less bluff leading edges promote lower energy dissipation, producing smaller separation bubbles and inducing consequently peaks closer to the leading edge. The point where the flow reattaches in rectangular cross-sections is located in a distance around *4.4D* from the leading edge [Saathoff and Melbourne, 1989], where *D* is the thickness of the cross-section, which in normalized dimensions corresponds to $\Delta x_R^*=0.44$, and considering the bluffness of the leading edge of a rectangular cross-section, this value can be regarded as a superior limit and a reference for other types of leading edges. As it can be noticed in Fig.13-14, all the values are situated indeed below that limit, which is reached only in the *NF* case, in the highest reduced wind velocity (*U/f.B=25*).

For the interpolation of the values presented by the distributions of Fig.13 and Fig.14, the use of an equation in the form of a *Weibull distribution*, Eq.4, impacted by a *bias* value $\tilde{C}p_0$ and normalized by its maximum value is proposed. The *bias* value is necessary to account for the residue of the decaying of the amplitude of fluctuation of the unsteady pressures, adjusting the curve to its minimum level. Through a weighted mean among the values assumed after the last inflection point, *0.1* was assumed as an initial value for $\tilde{C}p_0$.

$$C_p N(x^*) = \left[\frac{\gamma_{cp}}{\alpha_{cp}} \cdot \left(\frac{x_{cp}}{\alpha_{cp}} \right)^{\gamma_{cp}-1} . e^{-\left(\frac{x_{cp}}{\alpha_{cp}} \right)^{\gamma_{cp}}} + \tilde{C}_{p0} \right]_{\max=1} \tag{4}$$

where: γ_{cp} *is the shape parameter;* α_{cp} *is the scale parameter;* x_{cp} *is the x coordinate defined by* $x_{cp} = x^* + 1$*; e is the Euler's number.*

In addition to the *bias* value $\tilde{C}p_0$, the use of Eq.4 demands the definition of the parameters γ_{cp} and α_{cp}, which can be estimated in the same fashion it was done for the phase difference distribution in the previous section, by considering the normalized amplitude distributions $\tilde{C}pN$ presented in Fig.13 and Fig.14. The calculations should be conducted through an iterative procedure, getting the values of the parameters refined after each iteration, until the error of the approximations, calculated through least squares method, is minimized. The shape parameter γ_{cp} is evaluated, through *Maximum Likelihood Estimation* method, and by applying it in Eq.4 the values for the scale parameter α_{cp} are obtained. The results of the last iteration are presented in Table 1.

(a) γ_{cp}

$U/f.B$	5	10	15	20	25
NF torsion	3	2.2	2.15	2.2	2.2
NF heaving	2.85	2.7	2.8	2.9	3
CU torsion	1.9	1.55	1.3	1.3	1.6
CU heaving	1.8	1.8	1.95	2	2.2
CD torsion	3.8	3	2.3	2.1	2.2
CD heaving	3.7	2.5	2.1	2.1	2.2
SC torsion	3	2.05	2	2.2	2.1
SC heaving	3.5	2.3	2.5	2.3	1.5

(b) α_{cp}

$U/f.B$	5	10	15	20	25
NF torsion	0.34	0.43	0.48	0.53	0.6
NF heaving	0.32	0.42	0.47	0.5	0.55
CU torsion	0.17	0.2	0.27	0.32	0.39
CU heaving	0.2	0.26	0.29	0.3	0.32
CD torsion	0.3	0.28	0.3	0.33	0.38
CD heaving	0.3	0.3	0.3	0.29	0.32
SC torsion	0.26	0.25	0.24	0.2	0.24
SC heaving	0.26	0.21	0.19	0.17	0.14

Table 1 - Parameters for Eq.4

Although the shape parameter γ_{cp} presents some discrepancies, which with the increase of the wind velocity tend to oscillate in a range around the value of *2*, defining a *Rayleigh* distribution, it can be said that all models present similar patterns in both systems for both parameters, especially the scale parameter α_{cp}. Considering as a extrapolation that the unsteady pressures amplitude behaves as a *Rayleigh* distribution, the scale parameter α_{cp} can be regarded as the one which characterizes each leading edge in terms of unsteady pressure amplitude distribution.

The efficacy of Eq.4 can be verified by recalculating the aerodynamic derivatives of the four cases by using the amplitude distributions produced through it combined with the real phase difference distributions and finally comparing the results with the real values, calculated from wind tunnel tests data. Fig.15 presents the $\tilde{C}p(x^*)$ distributions obtained with Eq.4 for *NF* in torsion oscillation and Fig.16 the aerodynamic derivatives obtained for the 4 cases, compared with both real values and Theodorsen equation. The good agreement obtained in the comparisons provided by Fig.15 and Fig.16 confirms that Eq.4 is able to provide reasonable approximations, provided the right parameters are used.

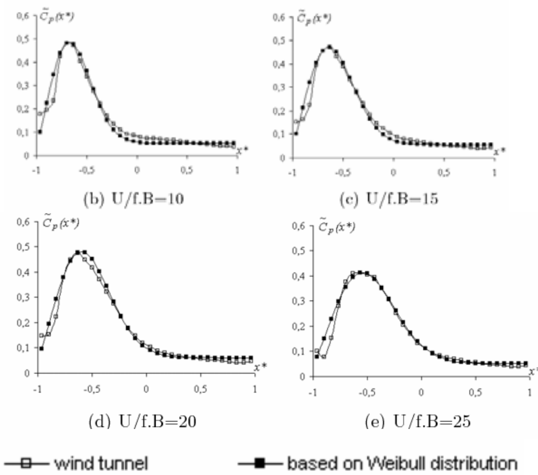

Figure 15: $\tilde{C}p(x^*)$ *distributions for NF in torsion obtained with Eq.4 and compared with wind tunnel test data*

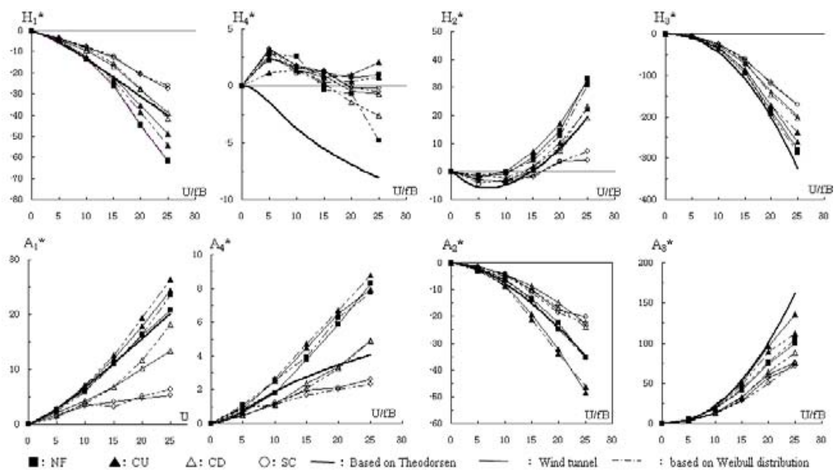

Figure 16: Derivatives - wind tunnel versus Eq.4

Final Analysis

The inverse of the parameter α_{cp} has its equivalent in the phase difference distribution, Eq.1, provided by the normalized wave half-length $\lambda/2$, which is given by the relation $\omega_\psi/2\pi$. A comparison between both values in the 4 geometries of leading edges for all reduced wind velocities indicates that they present similar tendencies and might be indeed comparable through a "proportionality relationship". In the search of this "proportionality relationship" the ratio between both values was evaluated for all configurations, showing a tendency towards the unity as γ_{cp} approaches π. So comparisons between the index γ_{cp}/α_{cp} multiplied by 2 with the value of ω_ψ show very good agreement, pointing to a strong relationship between phase difference $\psi(x^*)$ and amplitude $\tilde{C}p(x^*)$ distributions. This relationship is associated to the wave length and can be understood in the calculation framework proposed herein as an index inherent to each type of leading edge. Fig.17 shows this comparison for model NF in torsion and in heaving motions.

The aerodynamic derivatives of all models were evaluated by considering both the phase difference and the unsteady pressure distributions calculated through the approach proposed in this study, by using Eq.1 and Eq.4. The results are presented in Fig.18, showing good agreement with the real values for all aerodynamic derivatives, with the exception of some discrepancies in the approximations obtained for H_4^* derivative. The tendency presented by H_4^* in the approximations was to approach the Theodorsen equation, and this behavior is somehow expected for such a cross-section, having been already reported [Matsumoto, 1996].

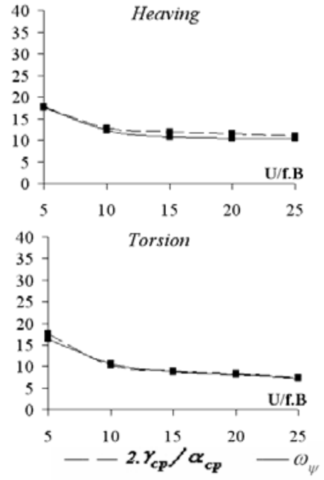

Figure 17: - Comparison between γ_{cp}/α_{cp} and ω_ψ for NF model

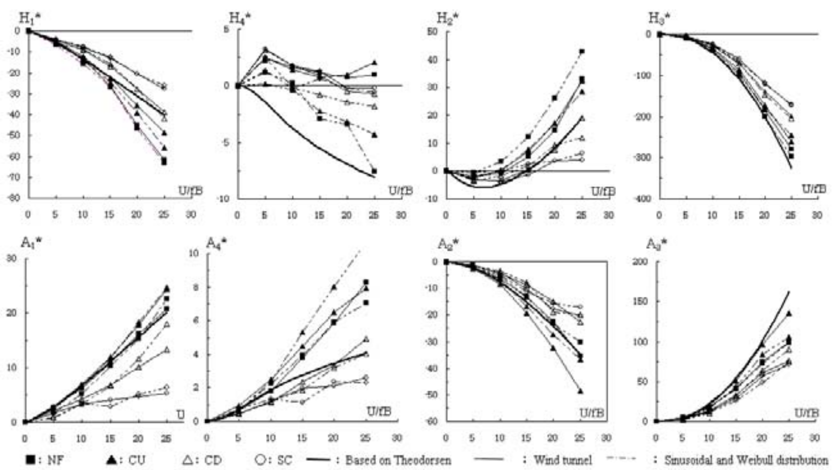

Figure 18: Derivatives - wind tunnel and sinusoidal equation with Weibull distribution

Conclusions

This study is part of a research in which generic formulations to be used in the estimation of the unsteady pressure characteristics of bluff bodies considering their geometric arrangements are being currently investigated. As a first step towards this objective, the formulations should be proved efficient in the reproduction of known distributions, so that the analyses presented herein were performed with the objective of confirming this ability, by reproducing the unsteady pressure characteristics of rectangular cross-sections with the use of empirical coefficients obtained through wind tunnel tests. The phase difference could be successfully approximated by a sinusoidal equation and the amplitude distribution was found to follow a Weibull distribution, being both equations interrelated through the wave length developed along the body. The efficacy was confirmed by comparing the aerodynamic derivatives calculated with the unsteady pressure characteristics reproduced with the formulation and the ones provided by wind tunnel experiments.

In this study empirical coefficients were applied, however analytical solution for these coefficients based on fluid mechanics concepts are expected as future works. Also, subsequent steps include the acquisition of the coefficients for different types of leading edges, considering also the impacts of geometric *singularities* along the body, as vertical plates and slots.

References

Kubo, Y., Hirata, K. (1990), “Aerodynamic responses and pressure function of shallow H-section cylinder”, Journal of Wind Engineering and Industrial Aerodynamics, 33, 123-130.;

Matsumoto, M. (1996), “Aerodynamic Damping of Prisms”, Journal of Wind Engineering and Industrial Aerodynamics, 59, 159-175.

Saathoff, P.J., Melbourne, W.H. (1989), “The generation of peak pressures in separated/reattaching flows”, Journal of Wind Engineering and Industrial Aerodynamics, 32, 121-134.

Silverstein, A. and Joyner, U. (1939), “Experimental verification of the theory or oscillating airfoils”, NACA Report No.673.

Tamura, T., Itoh, Y., Wada, A. and Kuwahara, K. (1995), “Numerical study of pressure fluctuations on a rectangular cylinder in aerodynamic oscillation”, Journal of Wind Engineering and Industrial Aerodynamics, 54, 239-250.